

# Neural mechanisms underlying catastrophic failure in human–machine interaction during aerial navigation

Sameer Saproo<sup>1,3</sup>, Victor Shih<sup>1</sup>, David C Jangraw<sup>2</sup> and Paul Sajda<sup>1,3</sup>

<sup>1</sup>Department of Biomedical Engineering, Columbia University, New York, USA

<sup>2</sup>National Institutes of Health, Bethesda, Maryland, USA

E-mail: [sameer.saproo@columbia.edu](mailto:sameer.saproo@columbia.edu) and [psajda@columbia.edu](mailto:psajda@columbia.edu)

Received 17 March 2016, revised 7 August 2016

Accepted for publication 10 August 2016


Published 5 October 2016



CrossMark

## Abstract

**Objective.** We investigated the neural correlates of workload buildup in a fine visuomotor task called the boundary avoidance task (BAT). The BAT has been known to induce naturally occurring failures of human–machine coupling in high performance aircraft that can potentially lead to a crash—these failures are termed pilot induced oscillations (PIOs). **Approach.** We recorded EEG and pupillometry data from human subjects engaged in a flight BAT simulated within a virtual 3D environment. **Main results.** We find that workload buildup in a BAT can be successfully decoded from oscillatory features in the electroencephalogram (EEG). Information in delta, theta, alpha, beta, and gamma spectral bands of the EEG all contribute to successful decoding, however gamma band activity with a lateralized somatosensory topography has the highest contribution, while theta band activity with a fronto-central topography has the most robust contribution in terms of real-world usability. We show that the output of the spectral decoder can be used to predict PIO susceptibility. We also find that workload buildup in the task induces pupil dilation, the magnitude of which is significantly correlated with the magnitude of the decoded EEG signals. These results suggest that PIOs may result from the dysregulation of cortical networks such as the locus coeruleus (LC)—anterior cingulate cortex (ACC) circuit. **Significance.** Our findings may generalize to similar control failures in other cases of tight man-machine coupling where gains and latencies in the control system must be inferred and compensated for by the human operators. A closed-loop intervention using neurophysiological decoding of workload buildup that targets the LC-ACC circuit may positively impact operator performance in such situations.

 Online supplementary data available from [stacks.iop.org/JNE/13/066005/mmedia](http://stacks.iop.org/JNE/13/066005/mmedia)

Keywords: motor control, flight, EEG, boundary avoidance task, pilot induced oscillations, pupillometry, rapid decision making

(Some figures may appear in colour only in the online journal)

## 1. Introduction

Superior human performance in complex tasks such as piloting a modern jet fighter or driving a Formula 1 car requires goal-directed navigation while operating within dynamic physical constraints or error margins. Such performance requires a careful balancing of cognitive resources, maximizing task engagement while keeping autonomic stress

<sup>3</sup> Authors to whom any correspondence should be addressed



Original content from this work may be used under the terms of the [Creative Commons Attribution 3.0 licence](https://creativecommons.org/licenses/by/3.0/). Any further distribution of this work must maintain attribution to the author(s) and the title of the work, journal citation and DOI.

responses in check. A failure to maintain this balance can result in catastrophic accidents. For instance, pilot-induced oscillations (PIO) are a dangerous flight characteristic that can spontaneously develop during periods of demanding task performance, e.g., when landing on the deck of a naval aircraft carrier, and can lead to loss of control and airframe damage (Hurt 1965).

Although the phenomenon of PIOs has been known in the flight community ever since the advent of manned flight, the underlying factors have not been completely understood. PIOs are defined as unstable oscillations in the longitudinal motion of an aircraft that are inadvertently caused by the pilot's own control input. Traditionally, PIOs have been attributed to non-optimal coupling between the pilot and the aircraft. Spontaneous dampened short-period oscillations are normal, but they can become dangerous if the pilot overcompensates for small control errors in a way that increases the amplitude of aircraft oscillations to dangerous levels. Moreover, a pilot's unfamiliarity with the 'feel' of the aircraft (e.g., during training or test flights of prototype airplanes) can increase the likelihood of a PIO (Hurt 1965).

Previous investigations into PIOs have suggested that an aggressive mindset, high pilot workload, and tight error margins could be contributing factors (Gray 2005, 2008). PIOs have been recreated in laboratory conditions using a 'boundary avoidance task' (BAT) paradigm, which entails gradually reducing the permitted margin of error while the pilot is attempting to closely track a complicated flight trajectory (Gray 2005, Warren 2006, Dotter 2007, Gray 2008). The BAT paradigm is thought to gradually increase a pilot's cognitive workload, arousal, and task engagement, until the cognitive conditions induce a catastrophic control failure, as in a PIO. However, what these cognitive conditions are, and how they mechanistically induce control failures, has not been determined so far.

We present the first neurophysiological study of PIOs, where we investigated neural factors underlying PIOs using a naturalistic 3D BAT paradigm while simultaneously recording EEG and pupillary activity, which was then used to build a predictive classifier that tracked PIO susceptibility. Our data suggest that heightened error monitoring and error sensitivity in the decision-making circuitry of the brain, along with increased arousal, are coincident with a higher probability of PIOs.

## 2. Methods

### 2.1. Experimental design and stimuli

We used NEDE (Jangraw *et al* 2014), a 3D virtual environment created using Unity game development platform (Unity Technologies, CA), to create a realistic visuomotor task. This task required maneuvering a high-speed virtual aircraft in first-person perspective through a series of equidistant glide boxes that defined a complex undulating trajectory (figure 1(A)). The environment was rendered on a 30 inch

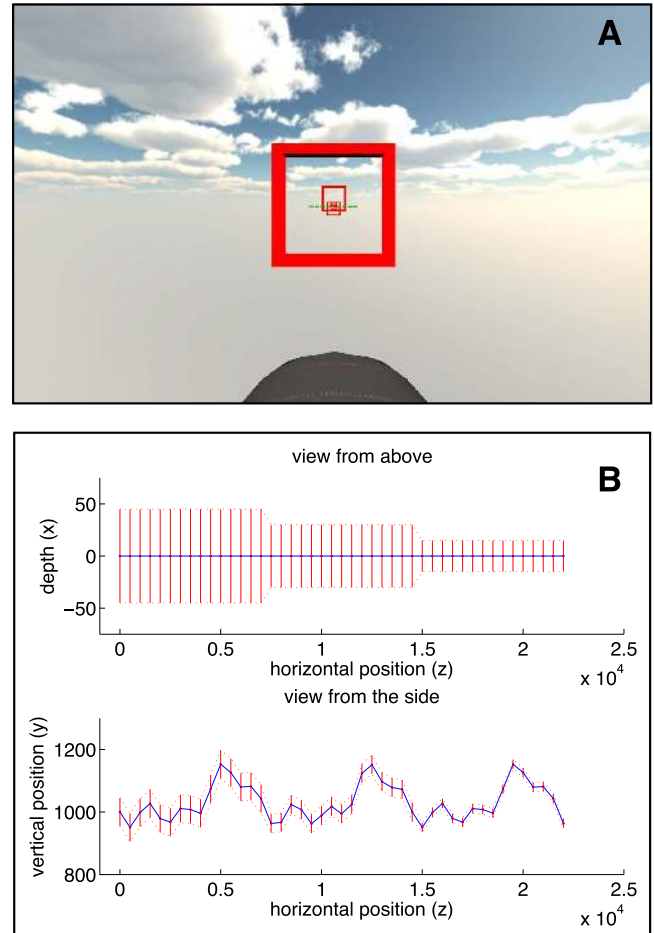


**Figure 1.** A) Screenshot of subject's view during 3D Boundary Avoidance Task (BAT) experiment. Red squares depict waypoint boundaries, while the dotted horizontal green line in the center shows the current heading of the virtual aircraft. B) Full flight trajectory with the position and the size of the glide boxes; solid blue line shows the mean path through the center of glide boxes, while solid red lines denote glide boxes. All dimensions are in meters. Virtual aircraft moved steadily along the z-axis at  $250 \text{ m s}^{-1}$  and could be controlled in y (pitch) axis via joystick input. See supplemental figure 1 [stacks.iop.org/JNE/13/066005/mmedia](https://stacks.iop.org/JNE/13/066005/mmedia) for the other glide path trajectory used in the experiment.

Apple Cinema HD display ( $1200 \times 800$ , 60 Hz) that subtended  $30 \times 23$  degrees of visual angle.

The virtual aircraft could be maneuvered in the pitch axis using a flight joystick (Attack 3 Joystick, Logitech S.A.), but with yaw and roll controls disabled. Glide boxes were placed every 500 m in the virtual environment, while the aircraft moved forward with a constant velocity of  $250 \text{ m s}^{-1}$ . Thus, a subject had to navigate through a glide box approximately every 2 s. The trajectory formed by glide boxes was modeled as a weighted sum of 3 sinusoids of varying periods and amplitudes in the pitch axis (figure 1(B), supplemental figure 1). Glide box boundaries were task critical; failure to navigate through even a single glide box ended the flight abruptly. The task difficulty was manipulated by decreasing the size of the glide boxes at regular intervals (30 s) during each trial. Therefore, the user-controlled flight during each trial (max 90 s) could be divided into 3 distinct epochs of identical glide

box trajectory but with steadily increasing difficulty; this is in consonance with previous 2D BAT investigations (Dotter 2007). Supplementary figure 1(A) shows a second glide path trajectory used in the experiment. Each trial started with 2 s of passive fixation (white cross in the middle of a blue screen) followed by 4 s of passive flight through the virtual environment towards the first glide box. The subject's joystick input had consequence only after the virtual aircraft had passed through the first glidebox in the trial.

The specific characteristics of the aircraft's response to control input play a critical role in the causation of PIOs, with a more oscillatory pitch response as well as response lag leading to higher chance of a PIO (Dotter 2007). Therefore, the pitch response of the virtual aircraft in our experiment incorporated both of these elements; an initial lag (200 ms or 300 ms) with a subsequent oscillatory movement of the aircraft in response to a step input of the joystick (supplemental figure 1). The maximum instantaneous and sustained pitch response was limited to 40 deg s<sup>-1</sup> and 24 deg s<sup>-1</sup> respectively.

## 2.2. Subjects

A total of 12 healthy human subjects (ages 19–33, all right handed, 4 females) with normal or corrected-to-normal vision participated in the study. Informed consent was obtained from all subjects in accordance with the guidelines of the Institutional Review Board at Columbia University. Subjects were provided with a set of written instructions about the task. They were also familiarized with the virtual aircraft controls by providing least 60–120 min of flying practice in the NEDE environment prior to the experiment, either on the same day as the experiment (3 subjects) or the previous day (9 subjects). Data from 3 subjects were discarded from final analysis due to system malfunction during the experiment or poor EEG quality, i.e., inability to get a sufficient number (>1) of neural independent components after artifact rejection (see data pre-processing section).

## 2.3. Data collection

During each trial, subjects' joystick input and the position of the aircraft were sampled at 60 Hz. In addition to motor behavior, subjects' neurophysiological activity was measured at 2048 Hz using an EEG system: Biosemi B.V. ActiveTwo AD-box, 64 Ag–AgCl active electrodes, 10–20 montage. All electrode offsets were below 40 mV at the beginning of the experiment. Gaze position and pupil size were recorded using an EyeLink 1000 eye tracker (SR Research, Ontario, Canada) at a 1000 Hz sampling frequency. The subject's head was stabilized during data collection using a chin and forehead rest. A 9-point calibration of the eye tracker was performed before each block of trials, and the subjects were instructed to not move their head between or during trials (they were provided regular breaks however). Note: stimulus delivery and behavior recording, EEG recording, and eye tracking were performed on 3 different computers simultaneously, with the respective data synced post-hoc (Jangraw *et al* 2014).

A total of 32, 40, or 48 flight runs were observed per subject, with the total experiment time not exceeding 1 h. Note that given 2 different pitch response delays and 2 different glide-path trajectories, each unique combination of delay and trajectory was run an equal number of times (e.g., 10 per combination, for a total of 40 trials per subject). This was done to maximize the probability of sampling pilot behavior relevant to PIOs given inter-subject variability in innate performance on the task. Furthermore, these changes in control parameters and flight trajectory across blocks of trials ensured that subjects had minimal learning or 'muscle memory' of the specific experimental parameters, and thus no steady increase in performance throughout the experiment.

## 2.4. Data pre-processing

All EEG and pupillometry data were analyzed using the EEGLAB toolbox (Delorme and Makeig 2004) in MATLAB (The MathWorks Inc., Natick, MA). The recorded EEG signals were first re-referenced to the average of all electrodes and then band-pass filtered to 0.5–100 Hz using a Hamming windowed FIR filter. The result was then notch filtered at 60 Hz to remove line noise, and finally down-sampled to 256 Hz. This pre-processing pipeline produced 'raw' datasets that contained signals from neural, ocular, and muscular sources, as well as non-physiological artifacts.

To isolate the purely neural component of the EEG data, we used the following procedure: we first reduced the dimensionality of the EEG data by reconstituting the data using only the top 20 principal components derived from principal component analysis (PCA). This dimensionality reduction step was included in order to better estimate the independent components associated with infrequent artifacts, as recommended by (Winkler *et al* 2011). Thereafter, an Independent component analysis (ICA) decomposition of the data was performed using the Infomax algorithm (Bell and Sejnowski 1995). We then used an ICA-based artifact removal algorithm called MARA (Winkler *et al* 2011) to remove ICs attributed to blinks, horizontal eye movements (HEOG), muscular activity (EMG), and any loose or highly noisy electrodes. MARA performs automatic IC classification using a linear classifier trained on time-series, spectrum, and scalp map features of a large dataset of labeled IC artifacts. MARA assigns each IC a probability of being an artifact; we removed components with probabilities above 0.5.

## 2.5. EEG data classification

The 64-channel EEG signals recorded during each trial were split into 1500 ms epochs that were centered at the onset of each stick movement. Thus, each epoch was construed as a unique data point for classification. We used spectral power as the classification feature; therefore, a spectrogram of the entire continuous data was computed using a sliding short time Fourier transform (STFT) with a 128 sample Hamming window and 64 samples of overlap between windows, yielding five 500 ms windows of frequency data for each electrode. For further analysis, frequencies were separated

into bands of interest: delta band consisted of frequencies 1–3 Hz, theta band 4–7 Hz, alpha band 8–15 Hz, beta band 16–31 Hz, and gamma band 32–55 Hz. Spectral information from 56–128 Hz was not used in the classifier.

Classification was performed either using the estimated spectral power in different frequency bands as features (delta only, theta only, alpha only, beta only, gamma only; 1 Hz resolution) or using the power from all frequency bands as features (all bands, figure 3; 1 Hz resolution). Each data point was given a class label according to the nearest boundary size at the time of stick movement during the trial. In one classification regime, which we call large versus medium/small (LvMS), the first class includes all stick movements made during navigation under large boundaries, and the second class includes all stick movements made during navigation under medium and small boundaries. In another classification regime, which we call time-on-task (ToT), data points generated only within large boundaries were sub-divided according to their temporal occurrence into two classes (first half or second half). Finally, the MvS classifier used the weight vector learned from the LvMS regime to classify medium versus small classes; this was done in order to show that the workload component (weight vector) was generalizable to different absolute boundary sizes. We used  $N$ -fold cross-validation to generate results, usually with both training and test data derived from the same subject, except in one case where leave-one-subject-out cross-validation was used to investigate whether the PIO classifier was generalizable to novel subjects.

**2.5.1. Classification algorithm.** The high dimensionality of data—there are 17 600 features per data point when using all frequency bands (1–55 Hz)—required the use of a recently developed algorithm FaSTGLZ (Conroy *et al* 2013), for efficient linear classification. FaSTGLZ classifies input data  $x \in \mathbb{R}^D$  with binary class labels  $y \in \{0, +1\}$  by using logistic regression to create a separating hyperplane in the feature space that is parameterized by a normal vector  $w = (w_1, \dots, w_D) \in \mathbb{R}^D$ . For the sake of simplicity, the classifier bias is estimated by incorporating a constant  $x_{D+1} = 1$  and bias term  $w_{D+1}$  into the classification.

The posterior probability of the class label  $y_i$  for each data point  $x_i$  is modeled as a sigmoid function:

$$p(y_i = 1 | x_i, w) = \frac{1}{1 + \exp(-x_i^T w)}. \quad (1)$$

For logistic regression, denoting  $p(y = 1 | x, w) = \mu(x^T w)$ , the negative log-likelihood is given by

$$\mathcal{L}(w) = -\sum_{i=1}^N y_i \log(\mu(x_i^T w)) + (1 - y_i) \log(1 - \mu(x_i^T w)). \quad (2)$$

A common problem with maximum-likelihood estimators is the severe over-fitting of high dimensional training data. FaSTGLZ mitigates such over-fitting by using a penalized likelihood method based on  $L_2$ -regularization that seeks to

minimize:

$$J(w) = \mathcal{L}(w) + \lambda w^T L w.$$

If the norm  $L$  is any symmetric positive semi-definite matrix and  $\lambda$  a real-valued scalar, then  $J(w)$  would be a convex function, which is optimized by FaSTGLZ using the ‘alternating direction method of multipliers’ (ADMMs) procedure. ADMM uses variable splitting to divide the main optimization into two simpler sub-procedures to minimize a differentiable objective and to solve a soft-thresholding operation. This allows the simultaneous training of high dimensional models across bootstraps, cross-validation folds, and permutation tests, thus considerably speeding up classifier learning. Note that all classifiers in our analyses were learned using 5-fold cross validation with 100 bootstraps for each fold. The optimal lambda values were chosen using a parameter sweep of 100 lambda values between  $1 \times 10^5$  and  $1 \times 10^{-5}$ ; the value that yielded the highest AUC was used for further analysis.

The resulting classifier assigns a set of weights to the feature space used to train the model, such that each multidimensional data-point is projected onto a scalar dimension where the two classes are maximally separated. The classifier features—spectral power of EEG signals—were z-scored across epochs before classification, and therefore the learned classifier weights can be interpreted as the normalized contribution of each frequency at each electrode to the discriminating hyper plane. A positive weight would imply that the classification feature is more correlated with low pilot workload (Larger boundary size) and a negative weight would imply a stronger correlation with higher pilot workload (smaller boundary size), therefore describing the direction of the change in spectral magnitude across boundary size. Furthermore, the entire set of classifier weights (frequency band  $\times$  time point  $\times$  electrode) can be localized on the scalp, thus showing the spatial and temporal signature of neural correlates of workload (figure 3).

We tested the statistical significance of the FaSTGLZ classifiers relative to chance (AUC = 0.5); by using FaSTGLZ’s built-in permutation setting to create two permutations per subject per band (with 5-fold cross-validation and 100 bootstraps in each permutation to find the average ‘null’ classifier performance). For each band, the distribution of the 18 ‘null’ classifiers was compared to the distribution of 9 ‘workload’ classifiers (there are 9 subjects), to compute a significance level using a t-test and an effect size using Cohen’s  $d$  (Cohen 1988). Note, that we limited to 2 permutations per subject as each computation took several hours to complete.

### 3. Results

The behavioral data show that our experimental paradigm elicited piloting behavior relevant to PIOs, i.e. there is an increase in the magnitude of PIO features with decreasing boundary size during the BAT (figure 2). Specifically, a reduction in boundary size led to quicker task failure (One-

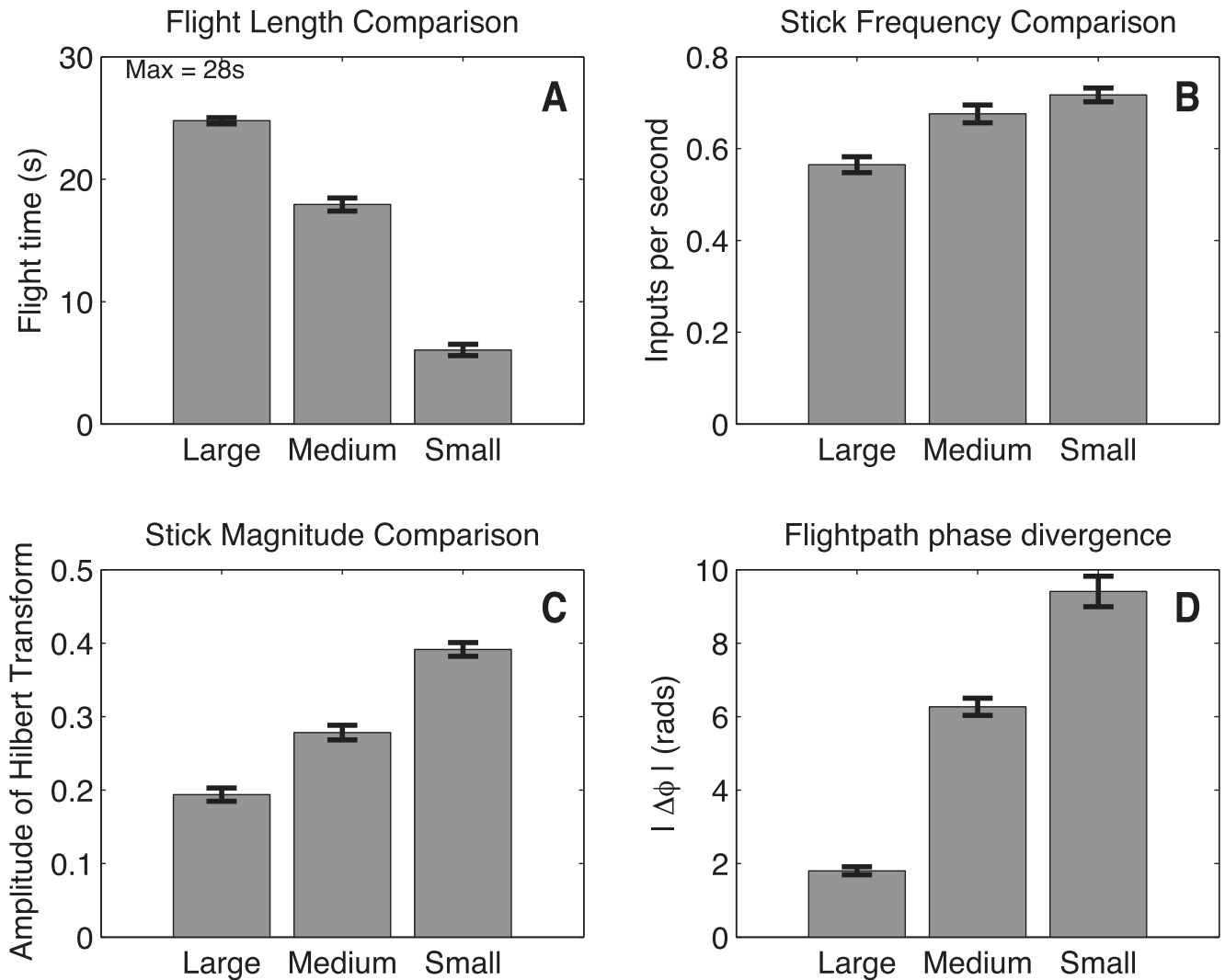


**Figure 2.** Four measures that demonstrate that the BAT paradigm elicited control behavior typical of PIOs; A) a reduction in boundary size led to a decrease in flight length before failure (missing a glide box), B) more frequent and C) larger joystick inputs, and D) a quicker increase in the phase divergence between the Hilbert transform of cumulative control input and current aircraft trajectory. Error-bars reflect mean  $\pm$  SEM across subjects (N=9).

way repeated-measured ANOVA;  $F(2, 16) = 185.3$ ,  $p < 0.001$ ), increased magnitude of joystick force ( $F(2, 16) = 63.59$ ,  $p < 0.001$ ), increased frequency of joystick input ( $F(2, 16) = 22.24$ ,  $p < 0.001$ ), and a rapid increase in the phase divergence between the input and the response ( $F(2, 16) = 25.37$ ,  $p < 0.001$ ). Here, the phase divergence was computed by taking the absolute the difference between the unwrapped phases of the Hilbert transform of the accumulated joystick input and the current aircraft heading.

We used the spectral power of stick-locked EEG signals (1500 ms around each stick movement) in different canonical frequency bands (delta, theta, alpha, beta, and gamma) as features to classify BAT-induced workload (classes: LvMS boundaries), and we observed above-chance classification accuracy (chance AUC = 0.5) for all subjects (figure 3(A), table 1). The choice of the size of the epoch was dictated by the asymptote of classification accuracy across different epoch sizes (supplemental figure 2). In order to dissociate the contribution of different frequency bands to workload

classification, we computed the classification accuracy for each band separately by filtering EEG signals to the respective band before classification (see Methods for specific frequencies for each band). The results show that the gamma band is the most informative band for classifying BAT-induced workload, as the gamma band classifier approximates the accuracy of a full spectrum classifier. This difference in classification accuracy does not seem to be a consequence of the higher dimensionality of the gamma band, as qualitatively similar results are produced when classifying using the average power in each band (supplemental figure 3). We also find that regularly sampling EEG signals (every 2 s) for classification did not have a significant qualitative difference from classifying stick-locked EEG signals (supplemental figure 4).

The scalp topology of the classifier weights for a full-spectrum classifier suggests that the contribution of delta, theta, and gamma band activity to workload classification is spatially localized. Delta and theta band based classifiers had

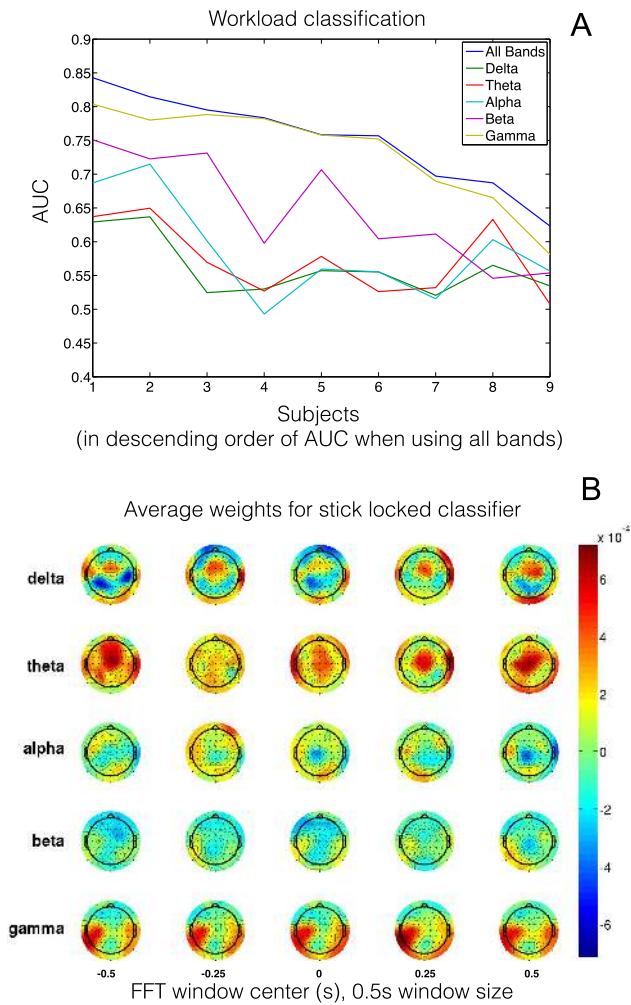


**Figure 3.** A) Area under the receiver operating characteristic curve (AUC) for all subjects (in descending order of ‘All Bands’ classifier AUC), when using information from all spectral bands for classification (‘All Bands’), as well as when using only individual bands (delta, theta, alpha, beta, or gamma). Classification was performed using 64-channel MARA-cleaned EEG signals — 1.5s epochs around each joystick movement — that were labeled according to the size of the nearest glide path boundary at the time of their generation. B) Subject-averaged scalp distribution of normalized weights for the classifier that best separated Large boundary from Medium and Small boundaries (scalp map corresponds to ‘Bands’ classifier in panel A). Delta and theta band activity from fronto-central electrodes, as well as significant gamma band activity from a lateralized somatosensory topography, seems most indicative of higher workload induced by smaller boundaries.

significant contributions from fronto-central sites, while gamma band modulation had a predominately lateralized somatosensory topography (figure 3(B)). Furthermore, the scalp topology for all frequency bands was robust to the variation in the temporal overlap of windows used to compute spectral power using a fast Fourier transform (see supplemental figure 5 for a classifier with higher temporal overlap).

We tested the robustness and the generalizability of classifiers from individual bands. We first estimated the statistical significance level and effect size in each band for the classification of MARA cleaned data (see methods). Figure 4

reports these results as uncorrected  $p$ -values and Cohen’s  $d$ . Classification results are highly significant, even when employing a stringent Bonferroni correction of  $p = 0.0083$  ( $p = 0.05/6$ ). The corresponding effect sizes are large, all greater than 0.8, which is a common rule of thumb with Cohen’s  $d$  (Cohen 1988).

When analyzing the effect of the MARA cleaning on the classification performance, we found that even though the theta band classifier does not produce the highest classification accuracy compared to the gamma band classifier, MARA-based artifact cleaning of raw EEG affected the theta-band classifier the least (figure 4). This result is not surprising because lower frequencies, such as theta, are known to be less susceptible to potentials from muscle activity (Whitham *et al* 2007). Therefore, fronto-central theta activity might prove to be the best indicator of workload in an operational scenario (i.e., while flying a real fighter plane), due to the significant contamination of EEG signals with EMG signals. Similarly, training the classifier with data from non-test subjects (hold-one-subject-out cross-validation) impacted the accuracy of theta band classifier the least, further attesting to its generalizability (figure 5). That said, including lateralized gamma band signals in a real-world classifier might prove to be advantageous as they could reflect increased grip on the joystick that is indicative of task-related stress (Goncharova *et al* 2003). In addition, it should be noted that sampling joystick-locked events has a tendency to produce overlapping epochs of data—with varying degrees of overlap—that can inflate classification accuracy due to non-independence issues. However, we found that in practice the impact on accuracy due to occasional non-independent samples was minimal (supplemental figure 6).

Workload can build up due to sustained focal attention required by the task, which would be unrelated to boundaries in the BAT scenario. However, we find that the contribution of ToT component to classifier performance for our data was not enough to explain the steadily increasing EEG signatures of workload in our BAT paradigm (figure 6, supplemental figure 7). Furthermore, the LvMS classifier (classes: large versus medium/small boundaries; data from medium and small boundaries were collapsed into a single class) could also reliably distinguish medium from small boundary conditions (MvS). This suggests that our assessed neural correlates (vector of weights normal to the classifying hyperplane) are independent of absolute boundaries and can reliably predict a continuum of workload states. More importantly, data suggest that neural correlates derived from laboratory BAT experiments can be effectively used to provide continuous feedback about pilot workload and PIO tendency in real-time (figure 7).

Although, we trained classifiers to discriminate EEG signals based on boundary size, we demonstrate that the classifier output can also track PIO tendency. We estimated PIO tendency by creating a metric: the amplitude of the Hilbert transform of band-passed stick movement (0.3–1.8 Hz, range that is typical of PIOs; Tian *et al* 2006, Rzuclidto 2007). We then separated the trials into 4 bands of increasing PIO tendency according to the magnitude of PIO

**Table 1.** Mean area-under-curve (AUC) values for workload classifiers (Classes: large versus medium/small boundaries) using different spectral content (mean ± SEM).

	All bands	Delta	Theta	Alpha	Beta	Gamma
Stick locked classifier	0.75 ± 0.02	0.56 ± 0.01	0.57 ± 0.02	0.59 ± 0.02	0.65 ± 0.03	0.73 ± 0.02
Regularly sampled classifier	0.75 ± 0.02	0.57 ± 0.01	0.58 ± 0.02	0.61 ± 0.02	0.66 ± 0.03	0.72 ± 0.03

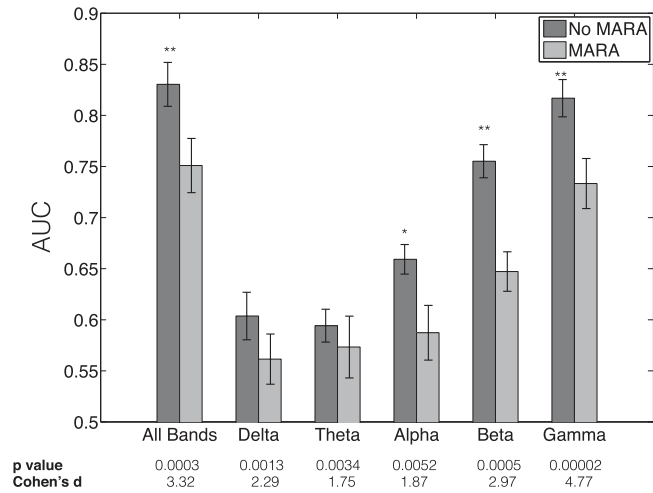


**Figure 4.** Effect of artifact removal, using MARA algorithm, on classification accuracy (Large vs Medium/Small) when using information all bands or when using individual bands. MARA algorithm classifies ICA components in the data as artifact based on a preexisting labeled set of artifactual ICs, including those for eye movements, muscle movements, and noisy electrodes. p values and Cohen's d show significance and effect size relative to chance classification performance for the MARA cleaned data. Error-bars reflect mean ± SEM across subjects. Paired t-tests are done to show the effect of the MARA cleaning on the classification performance (comparison of MARA vs. No MARA results); \* p<0.01, \*\* p<0.001. Figures 3, 5-9 show results from MARA cleaned data.

measure in the last 5 s of a trial, and compared highest to lowest band (Q1: band lower than 1st quartile; Q3: band higher than 3rd quartile). We find that there is a significant difference between time-averaged classifier output that leads up to a PIO event towards the end of the trial (Q3), compared to trials that did not end in a PIO (Q1), with the temporal trend showing steady divergence (figure 8).

In addition to EEG, we collected pupillometry data while the subjects performed the experimental task. Data show that subjects' pupils dilate with a decrease in boundary size (figure 9(A)), directly implicating mental load and arousal (Murphy et al 2011). We find a significant correlation between EEG-derived classifier output and pupil size for a full spectrum classifier (figure 9(B), one sample t-test;  $t(8) = -2.41, p = 0.043$ ). More importantly, we find a significant increase in the correlation between the output of the theta band classifier—with fronto-central topography—and the pupil size with a decrease in boundary size during BAT (large versus medium boundaries), suggesting a close anterior cingulate cortex (ACC)—locus coeruleus norepinephrine (ACC-LC-NE) interaction during induced workload buildup (One-way repeated-measures ANOVA;  $F(1, 8) = 8.08,$

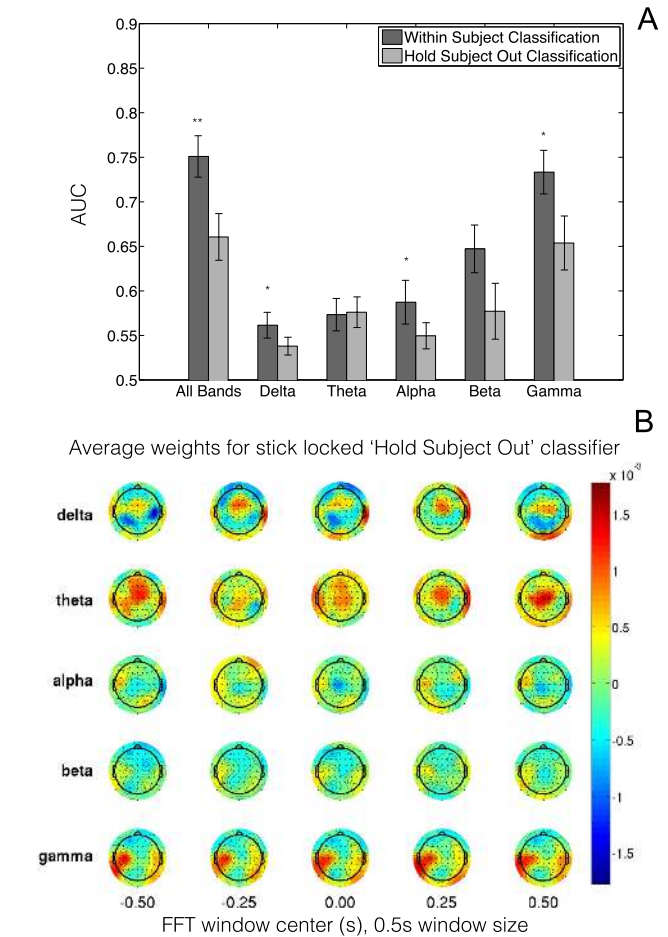


**Figure 5.** A) Comparison of classification accuracy (Large vs Medium/Small) when using 'Within subject' k-fold cross-validation or when using 'Hold Subject Out' cross-validation. Error-bars reflect mean ± SEM across subjects. Paired t-test; \* p<0.05, \*\* p<0.01 B) Subject-averaged scalp distribution of normalized weights for the classifying hyperplane that best separated Large boundary from Medium and Small boundaries for 'Hold Subject Out' classification (scalp map corresponds to 'All Bands' classifier in panel A).

$p = 0.022$ ). This change in correlation was not observed with the full-spectrum classifier ( $F(1, 8) = 0.02, p = 0.88$ ).

#### 4. Discussion

We performed the first neurophysiological investigation into the phenomenon of PIOs, using a BAT in a virtual reality environment. We find that our task is able to gradually induce cognitive workload that in some cases causes PIO-like behavior. Furthermore, we find robust EEG signatures of workload in different spatio-spectral bands, with fronto-

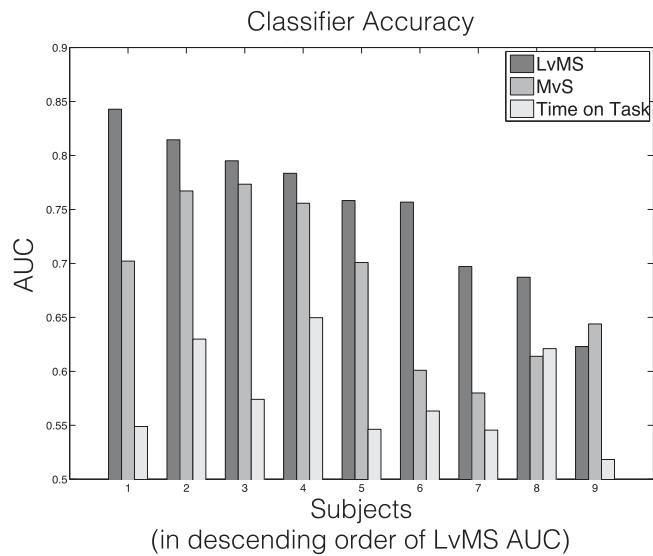


**Figure 6.** Subject-wise classification accuracy: LvMS, where data from Medium and Small boundaries were combined into a single training class, and the classifier learned to distinguish Large from Medium/Small boundary classes. MvS, used the weights learned from LvMS classifier and classified Medium vs Small boundary classes. Time on Task, when classifying data from the Large boundary class that is labeled according to temporal occurrence - first half or second half of flight within large boundaries.

central theta band the most robust, in terms of being differentiable from potential artifacts. We also find a significant correlation between this EEG activity and pupil dilation due to BAT induced workload. Below we discuss these results within the context of specific circuits in the brain and also possible broader implications of our findings.

Neural processes underlying cognitive workload have been studied extensively—especially using EEG measures—in behavioral contexts where workload is associated with working memory processes such as recall in n-back tasks (Brouwer *et al* 2012, Hogervorst *et al* 2014, Muhl *et al* 2014, Roy *et al* 2015). In contrast, our results are unique in that the workload induction in BAT should not be attributed to working memory, but to continuous error monitoring and calibration of motor output due to the very nature of the task. Furthermore, the steadily decreasing safety critical boundaries make the source of workload in BAT quite distinct from those in previous studied machine control tasks, such as driving (Dijksterhuis *et al* 2013) and flight cockpit management (Wilson and Russell 2003). As pilots navigate under tighter boundary conditions, the perception–action cycles become temporally shorter, which should require more cognitive resources and induce a subjective feeling of higher ‘workload’. Thus, a neural explanation of workload in BAT would primarily involve regions and circuits underlying error monitoring and cognitive control.

The encoding and regulation of error monitoring has typically been associated with the ACC, which is believed to be a key brain area for cognitive control and storing of predictive models of our environment (Tervo *et al* 2014). The region ACC is believed to be at least partially modulated by

the locus coeruleus, a tiny nucleus in the dorsal pons, regulating arousal levels in the brain via the neurotransmitter norepinephrine (Aston-Jones and Cohen 2005). The link between arousal state and task performance has been shown to be nonlinear (Aston-Jones and Cohen 2005, Gompf *et al* 2010). For example, the Yerkes–Dodson curve posits that a mid-level arousal state is optimal for task performance, though this ‘mid-level’ is highly task and context dependent. Therefore, the LC-ACC circuit is of particular interest in decision-making under dynamic constraints (e.g., flying an aircraft or driving a vehicle) since dynamically adapting motor control strategies based on assessment of current performance and upcoming task constraints is often key to optimal performance.

Recent work in animal models has shown a tight coupling between the LC- norepinephrine system (LC-NE) and the ACC when animals must dynamically switch between task-based models (Tervo *et al* 2014). Specifically, the rats in the experiment faced a computer opponent in a competitive virtual task, where the computer was programmed to counter-predict a rat’s behavior. When the LC-NE input to the ACC increased, the rats were less adept at incorporating environmental feedback into their internal model of choice and prediction. However, when the LC-NE input to ACC was suppressed, the rats were able to utilize feedback from the environment more effectively and therefore better model the computer’s counter prediction to increase their performance and reward.

Though we cannot directly measure LC-NE activity with scalp EEG, several studies have shown that pupil dilation can be used as a proxy for activity in the LC and thus provides some information of the state of arousal of an individual (Gompf *et al* 2010, Joshi *et al* 2016). ACC, on the other hand, is more accessible via EEG, with fronto-central theta activity having been identified as a correlate of ACC activation (Cavanagh and Frank 2014). Thus, by linking EEG activity with pupillary measures, one can potentially, non-invasively, infer the dynamics of the LC-ACC circuit during a complex and dynamic task.

Our results, therefore, can be interpreted within the context of the aforementioned study of LC-ACC interaction (Tervo *et al* 2014), and may provide a mechanistic explanation for PIOs. An increase in observed fronto-central theta band power, which in turn is correlated with pupil dilation in our study, could be an indication of the subject switching into a behavioral model associated with high workload state. This might suggest that in a cognitive state associated with high workload, there is an increase in LC-NE input to ACC, which might lead to the subjects sticking with their current internal model of aircraft control, even when the boundaries have changed. This sub-optimal control model might lead to PIOs in certain instances. In contrast, a better strategy would be to incorporate environmental feedback and switch to a different internal model of aircraft control that is better adapted to steering within narrow boundaries.

This interpretation of our results provides an interesting possibility for mitigating PIOs: since the LC-NE system is associated with arousal, using feedback from a hybrid BCI



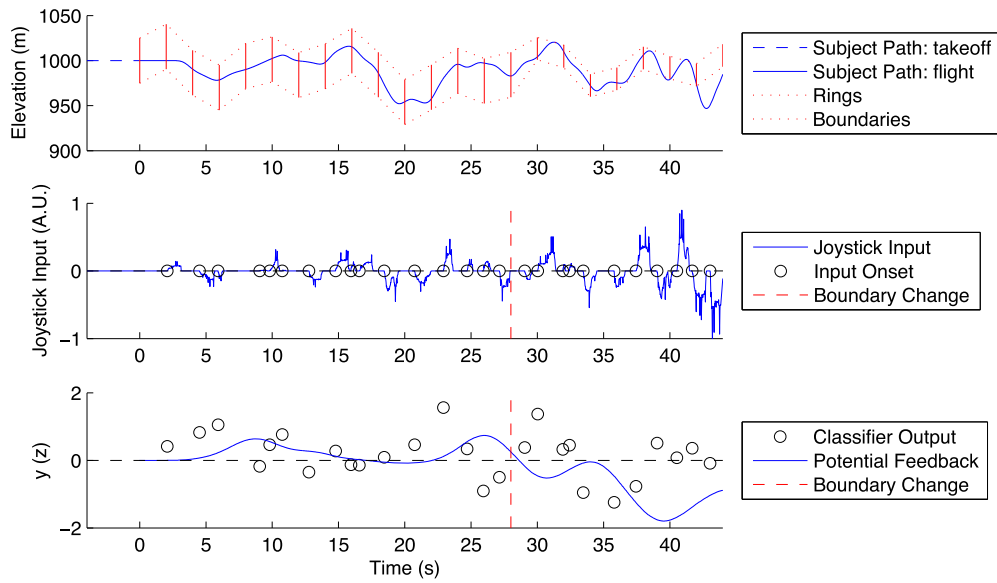


**Figure 7.** A representative trial flight showing the measured behavioral and neural markers across time. Top to bottom: Flight path, control stick movements, and z-scored classifier output  $y$ . Potential feedback to the pilot is constructed by interpolating and filtering classifier output (cubic spline interpolation, then 3rd order Butterworth filter with 0.1 Hz cutoff to smooth output over 10s)

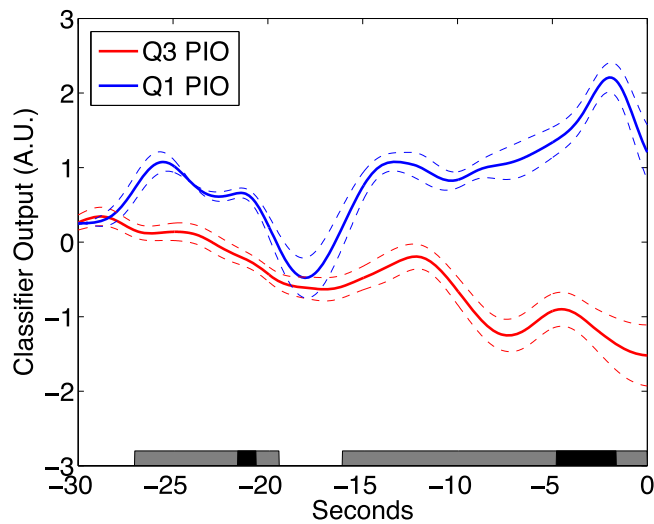


**Figure 8.** Output of workload classifier tracks PIO susceptibility in real-time. PIO susceptibility was estimated using a metric (0,1) based on joystick input (see Results). The last 5 seconds of each trial  $i$  that ended in the medium sized ring (40-60s after first ring is crossed) were analyzed for PIO susceptibility; maximum value  $M_i$  and time of maxima  $T_i$  were computed. ‘Q3 PIO’ reflects the interpolated classifier output in the 30 seconds leading up to  $T_i$  averaged over all trials where  $M_i > 0.75$ —i.e. greater than Q3. ‘Q1 PIO’ reflects similar information for all trials where  $M_i < 0.25$ —i.e. less than Q1. This data suggests that even though the LvMS classifier only learns to differentiate EEG signals from different boundary conditions during trials, it can also differentiate piloting behavior. Note that data from -5s to 0s in the figure is guaranteed to reflect classifier output generated only within Medium glide path boundaries. Error-bars reflect mean  $\pm$  SEM across subjects. Bottom band (gray) shows time-points where a paired t-test indicated significant difference between the two curves ( $p < 0.05$ ); black shows regions that passed Bonferroni correction (i.e.  $p < 0.00028$ ).

system (hBCI) to dynamically adjust arousal levels may regulate LC-NE input to the ACC, allowing updates to the internal model of the pilot based on the environmental feedback. For example, a hBCI that integrates pupillometry and EEG features could predict when a pilot is entering a state that will likely generate a PIO (as in figure 8, red curve), whereupon feedback, in the form of a continuous auditory stimulus with calming influence, could be delivered to reduce arousal level and thus reduce LC-NE input to ACC. We hypothesize that an optimally calibrated feedback loop would help regulate LC-ACC interaction, resulting in piloting behavior improvements.

Beyond cases of vehicular control, there is a large class of electronic games, such as the highly popular ‘flappy bird’, that resemble a BAT; the player controls a character moving at constant speed, avoiding obstacles and boundaries that become tighter as the game progresses. The objective in these games is to go as far along the course as possible. These games are known to be highly addictive, with the gamers repeatedly replaying the course from the beginning after a failure, trying to increase the distance they come along a course before failure. Although a recent attempt has been made to quantify the optimal parameters for such games such that they remain highly playable (Isaksen *et al* 2015), the cognitive factors underlying their addictive nature remains unknown. Our results from the BAT investigation suggests that not only does arousal level (as evidenced by pupil dilation) increase progressively as the boundaries decrease and therefore difficulty increases, but there is a dramatic increase in the cognitive workload due to task monitoring (as evidenced by theta band activity over fronto-central sites). This presents a peculiar hypothesis: perhaps the addictive nature of

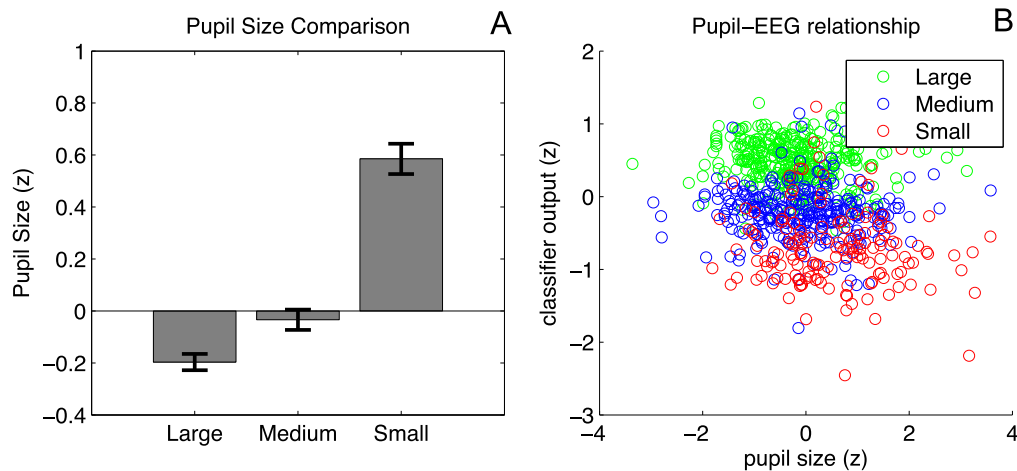


**Figure 9.** Pupillometry results. A) Data show an increase in pupil size (z-scored across each subject's data) with higher workload (smaller boundaries). B) The correlation between trial averaged classifier output (LvMS, full spectrum) and trial averaged pupil size, across all subjects (each datapoint represents a single trial). Overall correlation  $r = -0.1995$ ,  $SEM = 0.0764$ . 'Large' class correlation  $r = -0.0198$ , 'Small' class correlation  $r = -0.1210$ , difference n.s.

such games comes from the ability to progressively achieve higher arousal levels, as the subjects improve their ability to increase the ACC-LC coupling to move to the more optimal position along the Yerkes–Dodson curve. Indeed, our data show that the correlation between fronto-central theta band activity (stand in for ACC) and pupil dilation (stand in for LC activity) increases during the course of the experiment.

Finally, our results have relevance beyond the world of tracking physical boundaries as in gaming or vehicular navigation; humans frequently engage in sustained perception–decision–action loops that involve goal and error tracking under dynamic constraints. For example, a financial portfolio manager has to track changing market conditions and reallocate stocks so as to maximize portfolio value while managing risk within prescribed boundaries. Project managers must regularly track project progress and deal with exigencies so as to ensure high quality of work while avoiding unacceptable delays in completion. Viewed generally, these examples are illustrative of rapid decision-making that involves tracking optimal performance while avoiding frequently changing 'failure' boundaries. As with top-gun pilots, Formula 1 champions, top fund managers, and top project managers, the burning question is 'What neural markers differentiate stellar performance (and performers) from catastrophic failures under challenging conditions?' Our results suggest that the key insight may lay in the interaction of neural circuitry that is engaged in error monitoring, decision-making, and regulating arousal.

## Acknowledgments

The authors would like to thank Eric Pohlmeier and Mark Chevillet for their helpful comments and suggestions, and acknowledge Sona Roy and Wha-Yin Hsu for their assistance with data collection. The work was funded by the Defense Advanced Research Projects Agency (DARPA) and Army

Research Office (ARO) under grant number W911NF-11-1-0219, the Army Research Laboratory under Cooperative agreement number W911NF-10-2-0022 and the UK Economic and Social Research Council under grant number ES/L012995/1. The views and conclusions contained in this document are those of the authors and should not be interpreted as representing the official policies, either expressed or implied, of the US Government. The US Government is authorized to reproduce and distribute reprints for Government purposes notwithstanding any copyright notation herein.

## References

- Aston-Jones G and Cohen J D 2005 An integrative theory of locus coeruleus-norepinephrine function: adaptive gain and optimal performance *Annu. Rev. Neurosci.* **28** 403–50
- Bell A J and Sejnowski T J 1995 An information-maximization approach to blind separation and blind deconvolution *Neural Comput.* **7** 1129–59
- Brouwer A M, Hogervorst M A, van Erp J B, Heffelaar T, Zimmerman P H and Oostenveld R 2012 Estimating workload using EEG spectral power and ERPs in the *n*-back task *J. Neural Eng.* **9** 045008
- Cavanagh J F and Frank M J 2014 Frontal theta as a mechanism for cognitive control *Trends Cogn. Sci.* **18** 414–21
- Cohen J 1988 *Statistical Power Analysis for the Behavior Science* (London: Lawrence Erlbaum Association, APA)
- Conroy B R, Walz J M, Cheung B and Sajda P 2013 Fast simultaneous training of generalized linear models (FaSTGLZ) arXiv:1307.8430
- Delorme A and Makeig S 2004 EEGLAB: an open source toolbox for analysis of single-trial EEG dynamics including independent component analysis *J. Neurosci. Methods* **134** 9–21
- Dijksterhuis C, de Waard D, Brookhuis K A, Mulder B L and de Jong R 2013 Classifying visuomotor workload in a driving simulator using subject specific spatial brain patterns *Frontiers Neurosci.* **7** 149

- Dotter J D 2007 An analysis of aircraft handling quality data obtained from boundary avoidance tracking flight test techniques *Masters Thesis* Department of the Air Force Air University, Ohio
- Gompf H S, Mathai C, Fuller P M, Wood D A, Pedersen N P, Saper C B and Lu J 2010 Locus ceruleus and anterior cingulate cortex sustain wakefulness in a novel environment *J. Neurosci.* **30** 14543–51
- Goncharova I I, Mcfarland D J, Vaughan T M and Wolpaw J R 2003 EMG contamination of EEG: spectral and topographical characteristics *Clin. Neurophysiol.* **114** 1580–93
- Gray W 2005 Boundary avoidance tracking: a new pilot tracking model *AIAA Atmospheric Flight Mechanics Conf. Exhibit* (American Institute of Aeronautics and Astronautics)
- Gray W 2008 A generalized handling qualities flight test technique utilizing boundary avoidance tracking 2008 *U.S. Air Force T&E Days* (American Institute of Aeronautics and Astronautics)
- Hogervorst M A, Brouwer A M and van Erp J B 2014 Combining and comparing EEG, peripheral physiology and eye-related measures for the assessment of mental workload *Frontiers Neurosci.* **8** 322
- Hurt H H 1965 *Aerodynamics for Naval Aviators* (New York: Skyhorse Publishing)
- Isaksen A, Dan G and Nealen A 2015 Exploring game space using survival analysis *Foundations of Digital Games*
- Jangraw D C, Johri A, Gribetz M and Sajda P 2014 NEDE: an open-source scripting suite for developing experiments in 3D virtual environments *J. Neurosci. Methods* **235** 245–51
- Joshi S, Li Y, Kalwani R M and Gold J I 2016 Relationships between pupil diameter and neuronal activity in the locus coeruleus, colliculi, and cingulate cortex *Neuron* **89** 221–34
- Muhl C, Jeunet C and Lotte F 2014 EEG-based workload estimation across affective contexts *Frontiers Neurosci.* **8** 114
- Murphy P R, Robertson I H, Balsters J H and O'Connell R G 2011 Pupillometry and P3 index the locus coeruleus-noradrenergic arousal function in humans *Psychophysiology* **48** 1532–43
- Roy R N, Bonnet S, Charbonnier S, Jallon P and Campagne A 2015 A comparison of ERP spatial filtering methods for optimal mental workload estimation *Conf. Proc. IEEE Eng. Med. Biol. Soc.* **2015** 7254–7
- Rzucidlo P 2007 The detection of pilot-induced oscillations *Aviation* **11** 15–22
- Tervo D G, Proskurin M, Manakov M, Kabra M, Vollmer A, Branson K and Karpova A Y 2014 Behavioral variability through stochastic choice and its gating by anterior cingulate cortex *Cell* **159** 21–32
- Tian F-L, Gao Z-H and Yu Z-G 2006 Application of gaussian complex wavelet in PIO detection *Int. Congress of Aeronautical Sciences*
- Warren R D 2006 An investigation of the effects of boundary avoidance on pilot tracking *Masters Thesis* Department of the Air Force Air University, Ohio
- Whitham E M et al 2007 Scalp electrical recording during paralysis: quantitative evidence that EEG frequencies above 20 Hz are contaminated by EMG *Clin. Neurophysiol.* **118** 1877–88
- Wilson G F and Russell C A 2003 Real-time assessment of mental workload using psychophysiological measures and artificial neural networks *Hum. Factors* **45** 635–43
- Winkler I, Haufe S and Tangermann M 2011 Automatic classification of artifactual ICA-components for artifact removal in EEG signals *Behav. Brain Funct.* **7** 30